Saharan dust plume charging observed over the UK

Harrison, R. G. ORCID: https://orcid.org/0000-0003-0693-347X, Nicoll, K. A. ORCID: https://orcid.org/0000-0001-5580-6325, Marlton, G. J., Ryder, C. L. ORCID: https://orcid.org/0000-0002-9892-6113 and Bennett, A. J. (2018) Saharan dust plume charging observed over the UK. Environmental Research Letters, 13 (5). 054018. ISSN 1748-9326 doi: 10.1088/1748-9326/aabcd9 Available at https://centaur.reading.ac.uk/77604/

Saharan dust plume charging observed over the UK

Environmental Research Letters

LETTER

Saharan dust plume charging observed over the UK

R Giles Harrison[1,4], Keri A Nicoll[1,2], Graeme J Marlton[1], Claire L Ryder[1] and Alec J Bennett[2,3]

[1] Department of Meteorology, University of Reading, Reading, United Kingdom
[2] Department of Electrical and Electronic Engineering, Bath, University of Bath, United Kingdom
[3] Bristol Industrial and Research Associates Limited (Biral), Portishead, United Kingdom
[4] Author to whom any correspondence should be addressed.

E-mail: r.g.harrison@reading.ac.uk

Keywords: dust, meteorology, electrostatics

Supplementary material for this article is available online

OPEN ACCESS

RECEIVED
20 December 2017

REVISED
28 March 2018

ACCEPTED FOR PUBLICATION
10 April 2018

PUBLISHED
4 May 2018

Abstract

A plume of Saharan dust and Iberian smoke was carried across the southern UK on 16th October 2017, entrained into an Atlantic cyclone which had originated as Hurricane Ophelia. The dust plume aloft was widely noticed as it was sufficiently dense to redden the visual appearance of the sun. Time series of backscatter from ceilometers at Reading and Chilbolton show two plumes: one carried upwards to 2.5 km, and another below 800 m into the boundary layer, with a clear slot between. Steady descent of particles at about 50 cm s^{-1} continued throughout the morning, and coarse mode particles reached the surface. Plumes containing dust are frequently observed to be strongly charged, often through frictional effects. This plume passed over atmospheric electric field sensors at Bristol, Chilbolton and Reading. Consistent measurements at these three sites indicated negative plume charge. The lower edge plume charge density was (-8.0 ± 3.3) nC m^{-2}, which is several times greater than that typical for stratiform water clouds, implying an active *in situ* charge generation mechanism such as turbulent triboelectrification. A meteorological radiosonde measuring temperature and humidity was launched into the plume at 1412 UTC, specially instrumented with charge and turbulence sensors. This detected charge in the boundary layer and in the upper plume region, and strong turbulent mixing was observed throughout the atmosphere's lowest 4 km. The clear slot region, through which particles sedimented, was anomalously dry compared with modelled values, with water clouds forming intermittently in the air beneath. Electrical aspects of dust should be included in numerical models, particularly the charge-related effects on cloud microphysical properties, to accurately represent particle behaviour and transport.

1. Introduction

Aerosols are important constituents of planetary atmospheres because of their radiative and physical effects. In Earth's atmosphere, dust and smoke cause radiative effects from scattering or absorption of solar radiation (Highwood and Ryder 2014). It has long been appreciated that atmospheric dust can readily become electrically charged (Baddeley 1860), commonly by frictional interactions between colliding particles i.e. triboelectrification. The charge exchange varies with composition according to the *triboelectric series*, and many minerals charge negatively (e.g. Ferguson 2009). Strong charging has been observed in dust devils (Lorenz *et al* 2016, Harrison *et al* 2016), in Saharan dust from surface measurements (Ette 1971, Silva *et al* 2016, Katz *et al* 2018) and aloft (Nicoll *et al* 2011, Yair *et al* 2016); electric field enhancement is even thought to play a role in dust's initial release (Esposito *et al* 2016). Ordered electrical alignment of charged dust also affects how its radiative exchange properties should be represented in numerical models (Ulanowski *et al* 2007).

The introduction of dust and smoke into meteorological structures such as weather systems or small rotating structures (e.g. dust devils) can lead to transport away from the source region and mixing of independently emitted dust and smoke (Yang *et al* 2013). On 16th October 2017, long range transport associated with an Atlantic cyclone, which, at an earlier

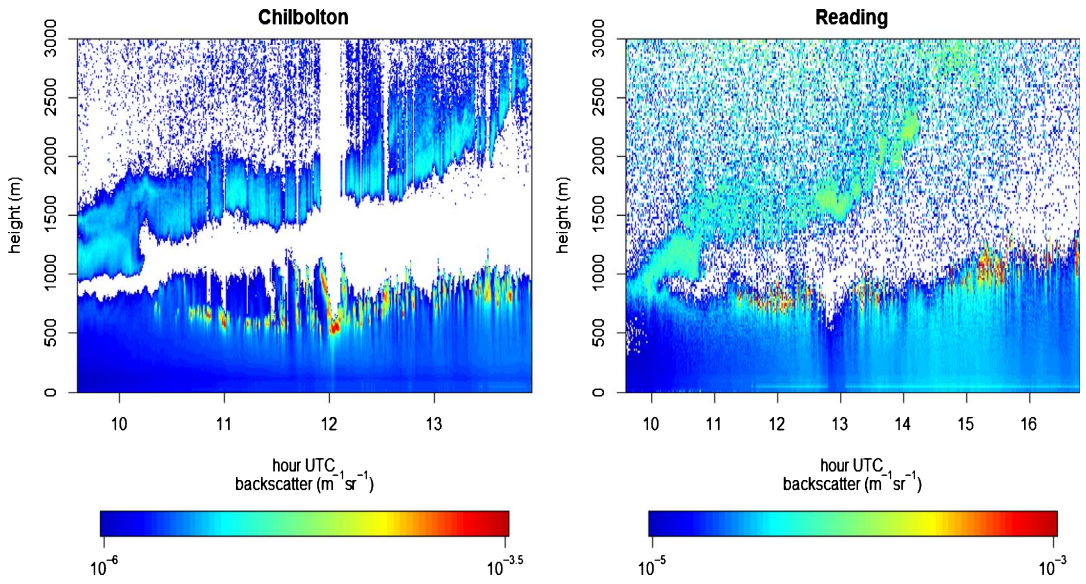

Figure 1. Time series of raw ceilometer backscatter profiles for (left panel), Chilbolton, Hampshire, and (right panel), Reading, Berkshire on 16th October 2017. (Chilbolton Observatory uses a Vaisala CL51 Ceilometer, and Reading a Vaisala CL31 device. The Chilbolton profiles were obtained every 30s and the Reading ones every 2s. White regions are where no laser return is generated, greater the instrument cut-off, due to beam attenuation by cloud beneath.)

stage in its development had formed Hurricane Ophelia (figure S1 available at stacks.iop.org/ERL/13/054018/mmedia), brought high aerosol loadings to the southern UK. Analysis of the back-trajectories (Stein *et al* 2015, figure S2) showed that the constituent particles originated in both the Sahara and the Iberia regions, bringing a combination of Saharan dust and smoke from Iberian forest fires. Some of the Saharan dust component reached the surface (figure S3), and the clearly-visible radiative effects from the particles aloft, causing reddening of the sun (figure S7), were widely noticed. The reddening of the sun arises from preferential scattering of blue light, as light is attenuated within the optically thick plume.

Here, electrical properties of the 16th October 2017 particle transport event are considered further, through a combination of surface measurements from multiple sites and a specially-instrumented balloon sounding.

2. Observations

The particle cloud from the Iberian and Saharan sources reached the southern UK on 16th October 2017, passing over well instrumented measurement sites, including those able to measure atmospheric electricity. Two of these sites, Chilbolton Observatory in Hampshire (51.13 °N, 1.43 °W), and Reading University Atmospheric Observatory in Berkshire (51.44 °N, 0.94 °W), were also operating laser ceilometers. These devices provide the vertical profile of backscatter from a vertically pointing infrared laser (wavelength 905 nm), and regular sampling provides time evolution of cloud and aerosol plumes passing over the measurement site. Figure 1 shows a time series of the backscatter profiles from the Chilbolton and Reading ceilometers (figure S1 gives the site locations). The water cloud at about 800 m generates strong backscatter returns. This strongly attenuates the beam, hence the plume region above the cloud is only intermittently revealed when there are gaps in the cloud layer. This shows an upper layer of particles between 1 and 2.5 km. At both sites, the upper plume layer rises during the day from about 10 UTC, whilst some material also enters the boundary layer. The region between the upper layer and the boundary layer causes little detectable backscatter. Because long range transport requires particles to be sustained at altitude despite rapid gravitational settling, this is interpreted as an upper plume above a clear region, through which particles fall into the boundary layer. (The back trajectory modelling, figure S2, further demonstrates that the different source regions can be associated with differents heights of the particles over the UK.)

2.1. Plume charging

During the plume's migration across the UK, three sites, at Bristol, Chilbolton and Reading, recorded the vertical electrical field beneath it (figure 2). These measurements are reported as the Potential Gradient (PG), following the usual atmospheric electricity sign convention: the PG is positive in fair weather conditions. All three sites show a prolonged dip in the PG from 7 UTC to 12 UTC, associated with the plume's passage. (Transient negative PG values due to rain at Bristol and Chilbolton have been removed.) At the two ceilometer-equipped sites, the reduction in PG evident in figure 2 coincides with a descending region

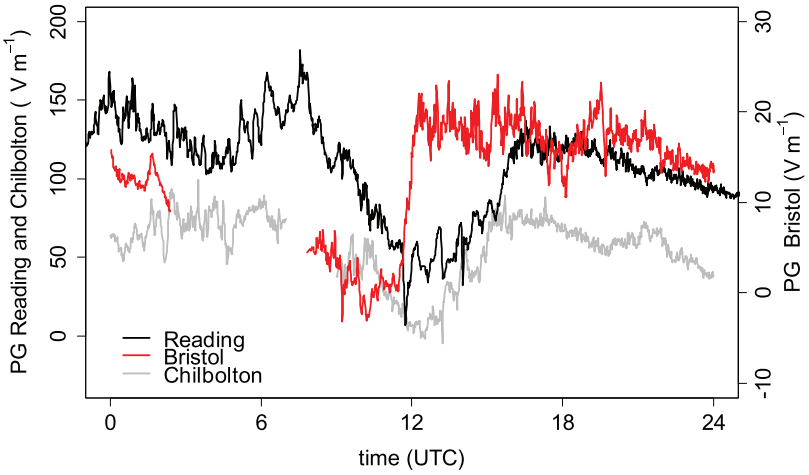

Figure 2. Potential gradient (PG) data for the day of the dust event on 16th October 2017 at the following UK sites: Bristol (red), Chilbolton (grey) and Reading (black). (All data are 1 minute averages. At Reading and Chilbolton CS110 and JCI131 field meters were used, both standardised to the same Reading Observatory JCI131. At Bristol, a Chubb JCI131 field mill was used, located on top of a building; values from Bristol are uncorrected for site distortion.)

in the boundary layer evident in figure 1, as the plume splits, to propagate both upwards and downwards (see also figure S4).

Further evidence exists for plume charging. At Chilbolton, an electrostatic lightning detector was in operation, which makes rapid (100 Hz) samples of the displacement current from an elevated spherical electrode above two toroidal electrodes (Bennett 2017). The power spectra from this instrument show increased broadband power between 11 UTC and 14 UTC, compared with the rest of the day (figure S5). This can be attributed to additional charge variability in the lower boundary layer during those times, which are coincident with the PG minimum at the site shown in figure 2. In addition, measurements from the upper spherical and lower toroidal electrodes showed extended periods of negative covariance during this time, consistent with charged particles or small hydrometeors impacting the electrodes (Bennett 2013). The negative covariance was most pronounced in the approximately 80 min prior to the PG minimum, between 1110 and 1235 UTC. At Reading, negative-going PG transients can be seen in the figure 2 data. Some of the transients will be associated with the downward progression of particles, and near-surface deposition is apparent in both the automatic visual range measurements and the PG measurements (see also figure S6).

Surface PG measurements are known to be influenced by charge above the site (Harrison *et al* 2017a), and the transient (timescale of minutes) and slower (timescales of hours) sustained decreases apparent in the surface PG (figure 2) at the three sites indicates negative charge in the plume. Closer inspection of the early part of the backscatter time series from Reading shows a descending structure in the backscatter, from 10 UTC–12 UTC. In figure 3, this has been identified using a narrow range of raw backscatter values, from $10^{-4.7}$ m^{-1} sr^{-1} and $10^{-4.5}$ m^{-1} sr^{-1}. (The conclusion about the descending nature of the plume is robust to the choice of backscatter range.) The PG measured beneath the descending plume shows a steady reduction with time, which is correlated with the height of the plume. This slow variation is typical of that occurring beneath negatively charged water clouds (Harrison *et al* 2017a), although the particle plume effect observed here is larger, which further supports the conclusion of negative charge in the plume.

2.2. Vertical structure

Figure 1 indicates the broad vertical structure of the plume above Chilbolton and Reading, of an upper region, a clear slot and particles within the boundary layer. To investigate this *in-situ*, an enhanced meteorological radiosonde package was launched into the plume from Reading at 1412 UTC. The radiosonde was a Vaisala RS92 carrying standard meteorological sensors for position, temperature, pressure and humidity, but with further sensors added for charge (Harrison *et al* 2017b) and turbulence (Marlton *et al* 2015). (Pictures of the sky during the balloon launch are given in figure S7.) Figure 4 shows the data obtained from the sounding. In figure 4(*a*), the timing of the sounding is marked on the backscatter time series, to show the remote sensing properties available during the balloon flight. Figure 4(*b*) shows the thermodynamic data obtained, plotted as dry bulb temperature (the air temperature) and dew point temperature (the temperature to which an air sample needs to be cooled to become saturated with water vapour), to show the water vapour content. In the clear slot between 1 and 2 km, the dewpoint depression is −35 °C, which is a much greater depression than that above and below, indicating that the clear slot contains dry air. The minimum relative humidity, at 1548 m, was 9%; at 1000 m and 2000 m it was 74% and 54% respectively.

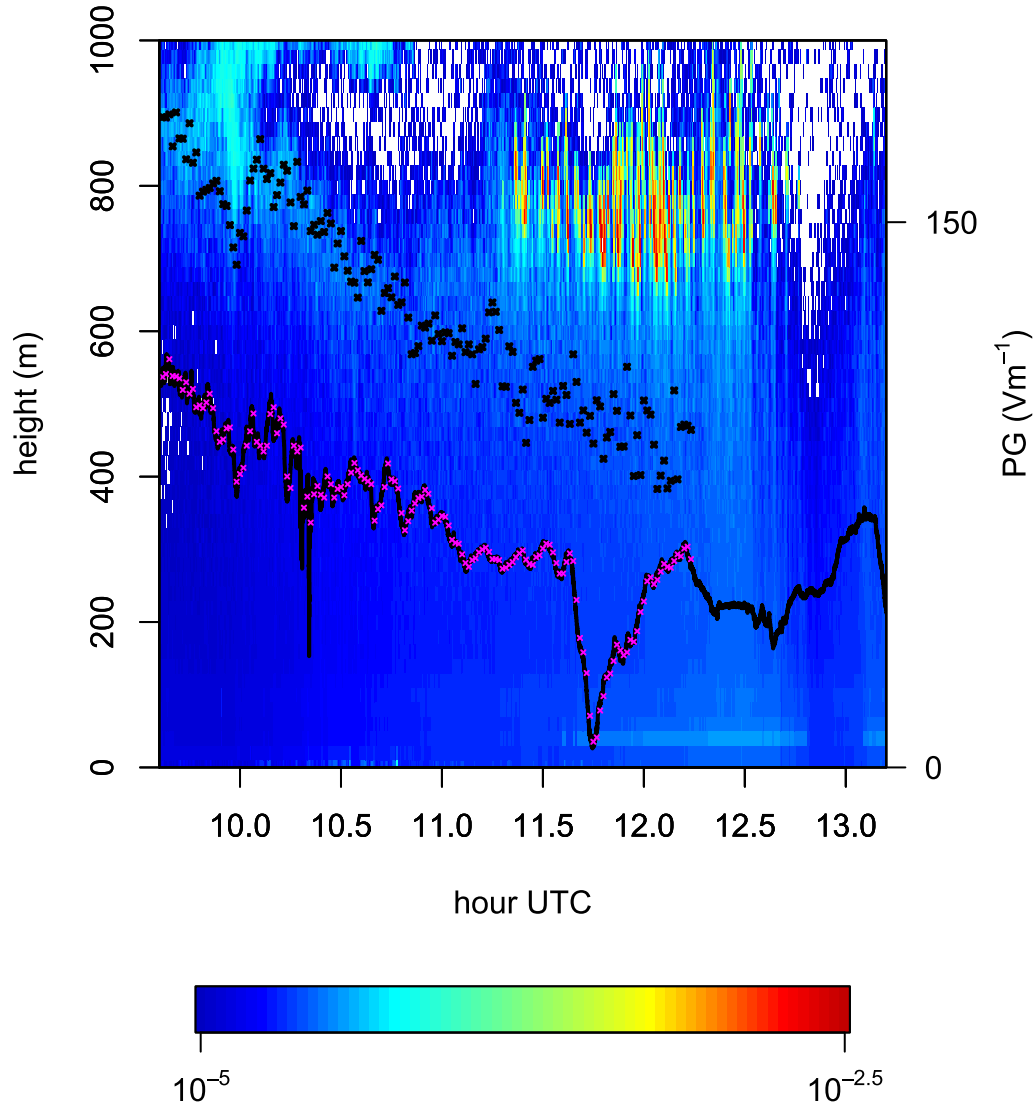

Figure 3. Time series of raw backscatter profiles obtained at Reading, during the plume progression. The descending edge of the plume is marked with black dots, selected by choosing a narrow range of backscatter values between $10^{-4.7}$ m^{-1} sr^{-1} and $10^{-4.5}$ m^{-1} sr^{-1}. The PG measured at the surface at Reading is also plotted, with the times corresponding to the plume edge values marked with pink crosses.

Figure 4(*c*) shows the charge profile, which shows charge below 1000 m altitude and centred around 3000 m. This is consistent with expectations of charging associated with the two principal regions of particles above and below the clear slot, with charge fluctuations considerably reduced in the clear slot. In figure 4(*d*), moderate turbulence is evident throughout the vertical profile, in the boundary layer the accelerometer standard deviation is 3–4.5 m s^{-2} which corresponds to an Eddy Dissipation Rate, a meteorological measure of turbulence intensity, of order 10^{-2} m^2 s^{-3} (Marlton *et al* 2015). Turbulence is therefore likely to be causing mixing of the particles, which is seen in figure 4(*a*) to occur throughout the boundary layer. Such boundary layer turbulence is likely to be caused by the interaction of substantial winds with ground objects. At 3 km, another region of turbulence is encountered of similar magnitude which coincides with the increased charge fluctuations seen in figure 4(*c*). Turbulence at this level is typically generated by wind shear, associated with the powerful jets present within extratropical cyclones.

2.3. Particle number concentration

Observations of the aerosol optical depth (AOD), aerosol layer depth and various assumptions about the aerosol optical properties and aerosol type allow calculations of the likely particle number concentration. AODs under non-cloudy skies are measured at AERosol RObotic NETwork (AERONET) sites by ground-based sun photometers (Holben *et al* 1998), provided at varying quality control levels: level 1.0 (unscreened), level 1.5 (cloud-screened) and level 2.0 (quality assured, post-deployment). At Chilbolton on 16 October, level 1.0 AODs of 0.27 and 0.19 at 500 nm were measured at 1514 UTC and 1527 UTC respectively. No data is available at level 1.5, indicating that the automatic algorithm detects high variability in the

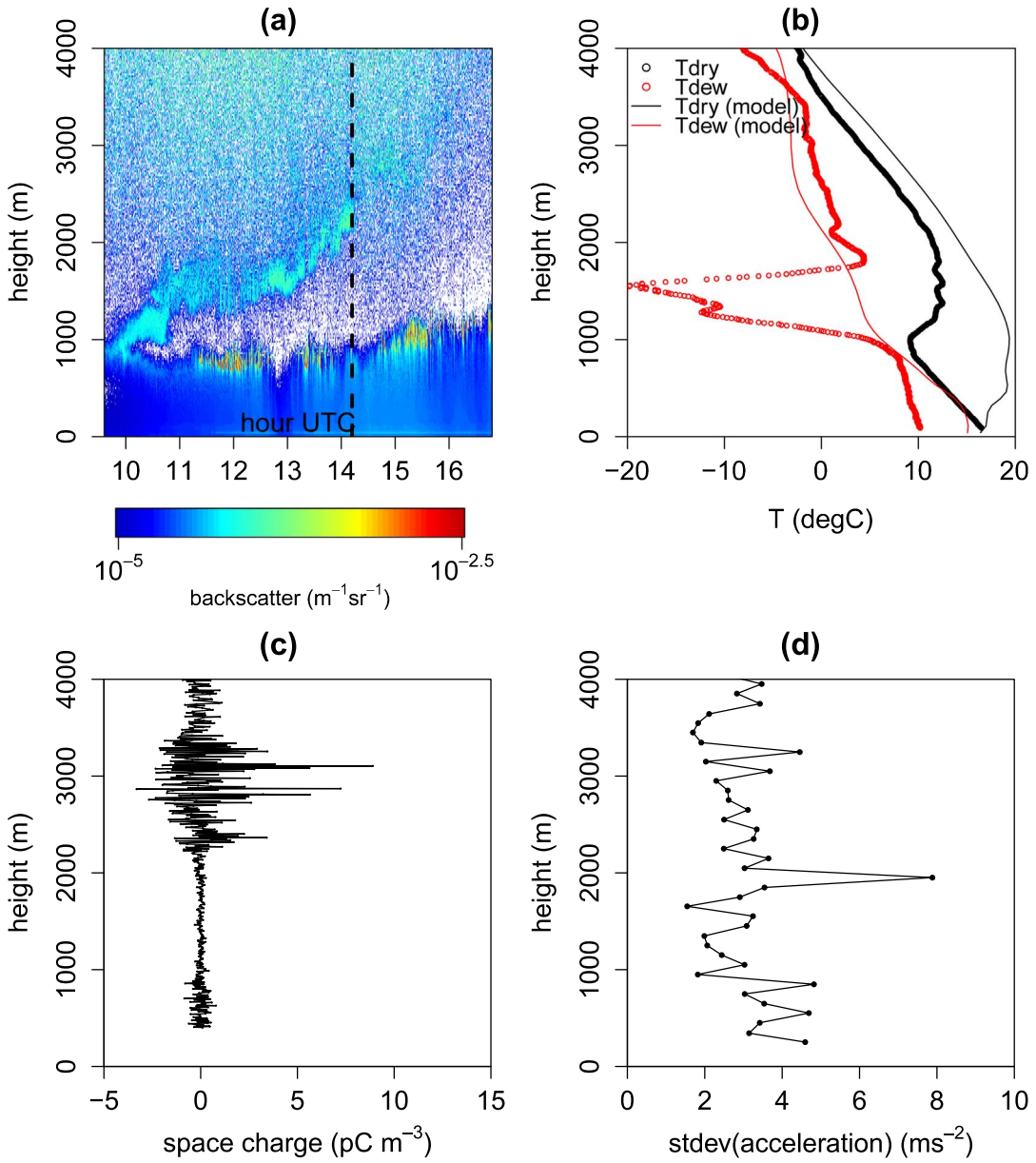

Figure 4. Measurements obtained from a balloon sounding from Reading, released at 1412 UTC. (*a*) shows the raw backscatter profiles around the time of the sounding. (*b*) shows the profile of measured air temperature (T_{dry}) and dew point temperature (T_{dew}), with the associated modelled profile (for 0.875°W, 51.370°N), from the European Centre (ECMWF) model initialised at 0000 UTC and 1200 UTC. (*c*) shows the charge profile determined by the balloon electrometer and (*d*) the standard deviation of the vertical acceleration encountered by the balloon package, calculated for vertical steps of 100 m.

AOD which it associates with cloud. It is, however likely that the level 1.0 AODs are reliable, since AERONET often diagnoses heavy aerosol loadings incorrectly as cloud (Omar *et al* 2013), and a nearby AERONET site at Bayfordbury (100 km to the northeast of Chilbolton and 60 km to the northeast of Reading) provides cloud-screened level 1.5 AODs of 0.41–0.46 between 0835 UTC and 1019 UTC on the same day. Satellite AOD retrievals from the MODerate Resolution Imaging Spectroradiometer (MODIS, not shown) indicate AODs varied between 0.2 and 0.7 within the warm sector containing the aerosol. Therefore we take an AOD of 0.3 as a reasonable best-estimate local value.

Using the method of Kaufman *et al* (2005) the aerosol mass path can be calculated by dividing the AOD by the aerosol Mass Extinction Coefficient (MEC), where values of around 0.4 m^2g^{-1} are typical for transported Saharan dust (e.g. Osborne *et al* 2008). Assuming the aerosol is entirely mineral dust, an AOD of 0.3 results in an aerosol mass path of 0.75 $g\,m^{-2}$, which can be combined with a layer depth of 1000 m (from the ceilometer observations) to give a mass concentration of 750 $\mu g\,m^{-3}$. Then, assuming typical transported mineral dust properties (density of 2.65 gm^{-3} (Rocha-Lima *et al* 2017), radius of 2 μm), spherical particle geometry and a monodisperse sample gives an individual particle volume of 3.4×10^{-17} m^3 and a number concentration of $\sim8\times10^{12}$ m^{-3}. Although this is a large value, the widely observed optical effects indicate an extensive

and dense particle cloud. Incorporating realistic uncertainties in the assumed parameters, including plume depth (500 m to 1300 m), MEC (0.23–1.0 gm^{-2}), AOD (0.2 to 0.7), and particle radius (1–10 μm) results in a range of number concentrations from 1×10^{10} to 3×10^{14} m^{-3}.

3. Discussion

Some physical aspects of the plume can be examined further quantitatively. Firstly, the rate of descent of the plume can be determined. Using a linear regression fit to the plume height in figure 3, the fall rate is (177 ± 4) m hr^{-1}, or ~50 cm s^{-1}. Assuming this is the particles' terminal velocity without additional meteorological influences and the particles have unit density, this can be used to determine the particle size. Using the relationship from Kasten (1968), a particle size of greater than 10 μm is indicated. Details of the particle composition and density will modify this result, as will the retarding effect of the particles' negative charge on their motion in the downward-directed electric field. Nevertheless it is clearly evident that the particles are coarse mode aerosol, from the material collected at the surface (e.g. figure S3). Secondly, the variation of plume height with surface PG allows the charge density on the lower plume edge to be retrieved, following the method of Harrison *et al* (2017a). This gives an estimate for the plume layer edge charge density of (-8.0 ± 3.3) nC m^{-2} (see also figure S8), many times greater than the typical charge density observed on the lower boundary of stratiform clouds. This indicates an active charging process, and a tribo-electric mechanism—frictional charging arising from particle collisions—would be consistent with the turbulence and particle sizes observed (Houghton *et al* 2013), rather than cloud boundary charging (Nicoll and Harrison 2016) associated with little mixing and the fair weather conduction current. Such self-generated charge has previously been observed in a dispersed volcanic plume over the UK (Harrison *et al* 2010). At altitudes of 2–3 km, a minimum in the air's electrical conductivity arising from the fall-off of surface ionising radiation with height and little cosmic ray ionisation, allows the particle charge to persist for longer than at higher or lower levels.

Beneath the clear slot, the ceilometer data shows that water clouds form from time to time, and it is possible that the cloud formation is influenced by the particles. Figure 5 investigates this more closely. Figure 5(*a*) shows that, at Reading, during a period when the cloud is intermittently generated, the profile of the backscatter (figure 5(*b*)), shows a maximum above the cloud base, with a fairly symmetrical vertical profile about this maximum. This is not inconsistent with material falling into a moist region, on which water condensed and carried downwards. The particles are sufficiently large that very little supersaturation would be needed for droplet formation and indeed, at the time of the sounding, the radiosonde data indicates that the upper boundary layer was not saturated (when the dewpoint and air temperatures would be equal). Figure 5(*c*) shows a period of descending water cloud observed above the Chilbolton site (between 11.9 and 12 UTC), for which the HALO Photonic Doppler lidar information is also available (figure 5(*d*)). This same period is associated with descending air, i.e. particles above would be falling into the cloud-forming region. Cloud formation at both sites can therefore be associated with falling particles.

A further interesting aspect is the dramatic humidity reduction observed in the sounding, within the clear slot. Figure 4(*b*) includes vertical profiles of dry bulb and dew point temperatures from the European Centre for Medium range Weather Forecast (ECMWF)'s operational high resolution deterministic forecast for the time and position of the radiosonde launch. The forecast was initialised at midday and run with a 0.125° (~14 km) horizontal resolution and 137 vertical model levels, using model cycle CY43R3. The model did not predict the dry slot, and over-predicted the air temperature. Although the model does consider some effects of tropospheric aerosols and dust, these are based on climatology of the seasonal aerosol distribution (Bozzo *et al* 2017) and therefore the particle transport by the extratropical cyclone and its subsequent effects would not be explicitly resolved. The particle plume may have contributed to both a reduction in solar radiation unresolved in the model and leading to greater cooling, and removal of moisture, as Saharan dust has sometimes been observed to have hygroscopic properties (Koehler *et al* 2009).

The strong observed negative charging of the particles is a further consideration in possible hygroscopic behaviour. For an electric field to polarise water vapour molecules, their thermal energy must first be overcome. The energy associated with polarisation of a molecule in a field of magnitude E is aE^2 where a is the polarizability (for water a is 1.6×10^{-40} C m^2 V^{-1}). To exceed the thermal energy kT at $T=273$ K (where k is Boltzmann's constant), E would typically be ~5 GV m^{-1}. Electric fields of this magnitude cannot be sustained without air breaking down. However, intense electric fields can exist over very short ranges, and clustering of molecules around a central atom to form molecular ions occurs as a result of such strong short-range fields. These effects extend to the collection of water molecules, leading to a close relationship between cluster ions and water vapour (Harrison and Aplin 2007). Although representing a cluster ion solely as a charged sphere is incomplete, the electrical influence of cluster ions on water vapour molecules is evident from calculating the electric field at the boundary of a unit-charged sphere of radius $r=1$ nm. This is given by $e/(4\pi\epsilon_0 r^2)$ with e the elementary charge and ϵ_0 the permittivity of free space, from which the boundary field is 4.5 GV m^{-1}. Water cluster ions are well-known

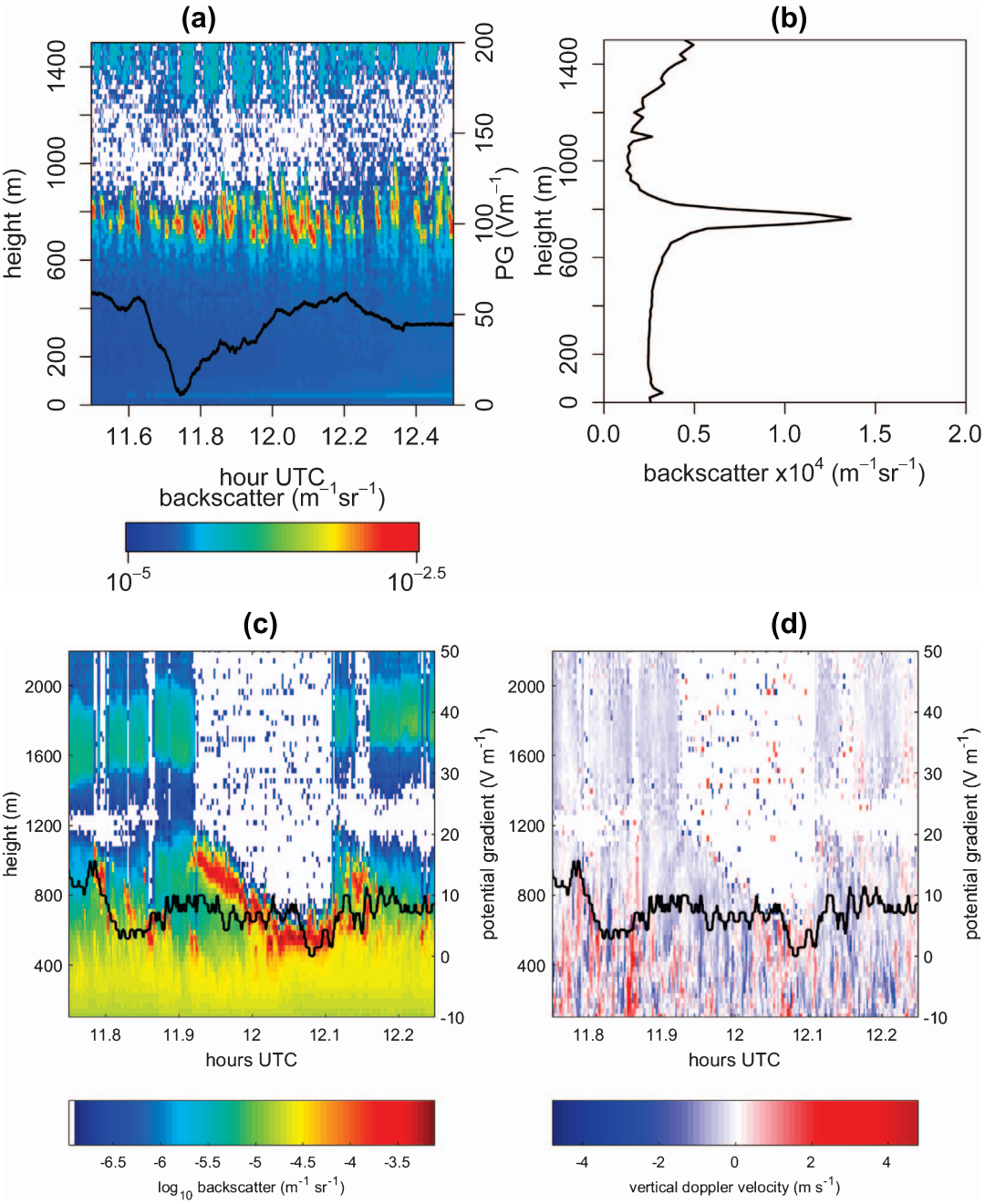

Figure 5. Time series of raw backscatter profile for Reading (*a*), and (*b*) the median profile during the same interval as shown in (*a*). The backscatter profile time series for Chilbolton is shown in (*c*), with the simultaneous Doppler lidar in (*d*). (*a*), (*c*), and (*d*) also include the simultaneous PG measurements for the site concerned.

to occur throughout the lower atmosphere (Hõrrak *et al* 2000). In the case of charged Saharan dust, which has a highly angular structure due to its mechanical generation (see figure S3), short range intense electric fields at a particle's surface will be inevitable. The observed charging of the plume may therefore contribute further to its hygroscopic nature.

Coarse mode mineral dust particles are also consistently observed to be transported over greater distances than can be explained by settling velocity theory (Ryder *et al* 2013, Weinzierl *et al* 2017, Gasteiger *et al* 2017). Further, both climate and numerical weather prediction models are unable to accurately represent dust size distributions (Evan *et al* 2014, Ansmann *et al* 2017, Kok *et al* 2017), which has ramifications for dust radiative effects and components of the climate system impacted by dust. These new observations of charging in long-range particle transport indicate that electrical effects need to be fully considered, as they may help to explain the unexpected prevalence of coarse dust particles in observations.

4. Conclusion

A 'red sun' event on 16th October 2017 was caused by atmospheric optical effects associated with the transport of Iberian smoke and Saharan dust to the UK, in a weather system inheriting the remnants of Hurricane Ophelia. In common with many other dusts and smokes, the dust plume was electrically charged. Quantitative estimates of the charging indicate that a process more active than fair weather cloud-edge charging was occurring. The denseness of the plume aloft evident from the associated optical effects, combined with strong turbulent mixing, suggests that triboelectric processes provided the charging observed.

The specially-instrumented radiosonde ascent deployed in response to the event provided direct *in situ* evidence of the plume charging, in the boundary layer and in the upper region of the plume. Between these two regions the air was anomalously dry and below this, water clouds formed intermittently. With the downward motion observed, water vapour was transported into the cloud-forming region beneath.

Aerosol is a key component in the planetary radiative balance, with dust a particularly variable aspect. Whilst electrical properties of dust have long been observed, its electrical effects are not considered in atmospheric numerical models and should be accounted for to give accurate representation of the associated microphysical processes and their impacts on long-range transport.

Acknowledgments

The authors thank Martin Airey for assistance with the balloon launch, James Gilmore for data processing and the Chilbolton PG data, James Matthews for providing the Bristol PG data and Helen Dacre for discussions. Balloon sensor development work was funded by the Natural Environment Research Council (NERC), Grant No. NE/P003362/1 (VOLCLAB). K.A.N. and C.L.R acknowledge NERC support through Independent Research Fellowships (NE/L011514/1, NE/L011514/2 and NE/M018288/1). NOAA's Air Resources Laboratory (ARL) is acknowledged for the provision of the HYSPLIT transport and dispersion model and/or READY website (www.ready.noaa.gov) used in this publication. The ECMWF forecast model data was obtained from the ECMWF MARS archive. The Halo Photonics lidar data at Chilbolton used in figures 5(*c*) and (*d*) was provided by Judith Jeffrey as was the CL51 data. The CS110 field mill and SWS-200 present weather sensor in temporary use at Reading during October 2017 were funded by the UAE research programme for rain enhancement science under grant 'Electrical aspects of rainfall generation'. We also thank I Woodhouse, J Agnew, J Jeffery and Z Ulanowski for their effort in establishing and maintaining AERONET Chilbolton and Bayfordbury sites.

ORCID iDs

R Giles Harrison https://orcid.org/0000-0003-0693-347X
Keri A Nicoll https://orcid.org/0000-0001-5580-6325
Graeme J Marlton https://orcid.org/0000-0002-8466-6779
Claire L Ryder https://orcid.org/0000-0002-9892-6113
Alec J Bennett https://orcid.org/0000-0001-8895-6418

References

Ansmann A *et al* 2017 Profiling of Saharan dust from the Caribbean to western Africa—Part 2: Shipborne lidar measurements versus forecasts *Atmos. Chem. Phys.* **17** 14987–5006
Baddeley P F H 1860 *Whirlwinds and Dust-Storms of India* (London: Bell and Daldy)
Bennett A J 2017 Electrostatic thunderstorm detection *Weather* **72** 51–4
Bennett A J 2013 Identification and ranging of lightning flashes using co-located antennas of different geometry *Meas. Sci. Technol.* **24** 125801
Bozzo A, Benedetti A, Remy S, Bechtold P, Rodwell M J and Morcrette J J 2017 *Implementation of a CAMS-based aerosol climatology in the IFS.* ECMWF Technical Memorandum No. 801
Esposito F *et al* 2016 The role of the atmospheric electric field in the dust-lifting process *Geophys. Res. Lett.* **43** 5501–8
Ette A I I 1971 The effect of the Harmattan dust on atmospheric electric parameters *J. Atmos. Terr. Phys.* **33** 295–300
Evan A T, Flamant C, Fiedler S and Doherty O 2014 An analysis of aeolian dust in climate models *Geophys. Res. Lett.* **41** 5996–6001
Ferguson D N 2009 A basic triboelectric series for heavy minerals from inductive electrostatic separation behaviour *Proc. 7th Int. Heavy Minerals Conference* (South Africa) pp 129–34
Gasteiger J, Groß S, Sauer D, Haarig M, Ansmann A and Weinzierl B 2017 Particle settling and vertical mixing in the saharan air layer as seen from an integrated model, lidar, and *in situ* perspective *Atmos. Chem. Phys.* **17** 297–311
Harrison R G and Aplin K L 2007 Water vapour changes and atmospheric cluster ions *Atmos. Res.* **85** 199–208
Harrison R G, Nicoll K A, Ulanowski Z and Mather T A 2010 Self-charging of the Eyjafjallajökull volcanic ash plume *Environ. Res. Lett.* **5** 024004
Harrison R G *et al* 2016 Applications of electrified dust and dust devil electrodynamics to Martian atmospheric electricity *Space Sci. Rev.* **203** 299–345
Harrison R G, Nicoll K A and Aplin K L 2017a Evaluating stratiform cloud base charge remotely *Geophys. Res. Lett.* **44** 6407–12
Harrison R G, Marlton G J, Nicoll K A, Airey M W and Williams P D 2017b Note: A self-calibrating wide range electrometer for in-cloud measurements *Rev. Sci. Instrum.* **88** 126109
Highwood E J and Ryder C L 2014 Radiative effects of dust *Mineral Dust: A Key Player in the Earth System* ed P Knippertz and J B Stuut 1st edn (Dordrecht: Springer) pp 267–283
Hõrrak U, Salm J and Tammet H 2000 Statistical characterization of air ion mobility spectra at Tahkuse observatory: classification of air ions *J. Geophys. Res. Atmos* **105** 9291–302
Houghton I M P, Aplin K L and Nicoll K A 2013 Triboelectric charging of volcanic ash from the 2011 Grímsvötn eruption *Phys. Rev. Lett.* **111** 118501
Holben B N *et al* 1998 AERONET—A federated instrument network and data archive for aerosol characterization *Remote Sens. Environ.* **66** 1–16

Kasten F 1968 Falling speed of aerosol particles *J. App. Meteor.* **7** 944

Katz S, Yair Y, Price C, Yaniv R, Silber I, Lynn B and Ziv B 2018 Electrical properties of the 8–12th September, 2015 massive dust outbreak over the Levant *Atmos. Res.* **201** 218–25

Kaufman Y J, Koren I, Remer L A, Tanré D, Ginoux P and Fan S 2005 Dust transport and deposition observed from the terra-moderate resolution imaging spectroradiometer (MODIS) spacecraft over the Atlantic Ocean *J. Geophys. Res.* **110** D10S12

Koehler K A, Kreidenweis S M, DeMott P J, Petters M D, Prenni A J and Carrico C M 2009 Hygroscopicity and cloud droplet activation of mineral dust aerosol *Geophys. Res. Lett.* **36** L08805

Kok J, Ridley D A, Zhou Q, Miller R L, Zhao C, Heald C L, Ward D S, Albani S and Haustein K 2017 Smaller desert dust cooling effect estimated from analysis of dust size and abundance *Nat. Geosci.* **10** 274–8

Lorenz R D, Neakrase L D V, Anderson J P, Harrison R G and Nicoll K A 2016 Point discharge current measurements beneath dust devils *J. Atmos. Sol. Terr. Phys.* **150–151** 55–60

Marlton G J, Harrison R G, Nicoll K A and Williams P D 2015 Note: A balloon-borne accelerometer technique for measuring atmospheric turbulence *Rev. Sci. Instrum.* 016109

Nicoll K A, Harrison R G and Ulanowski Z 2011 Observations of Saharan dust layer electrification *Environ. Res. Lett.* **6** 014001

Nicoll K A and Harrison R G 2016 Stratiform cloud electrification: comparison of theory with multiple in-cloud measurements *Q. J. R. Meteorol. Soc.* **142** 2679–91

Omar A H, Winker D M, Tackett J L, Giles D M, Kar J, Liu Z, Vaughan M A, Powell K A and Trepte C R 2013 CALIOP and AERONET aerosol optical depth comparisons: one size fits none *J. Geophys. Res.* **118** 4748–66

Osborne S R, Johnson B T, Haywood J M, Baran A M, Harrison M A J and McConnell C L 2008 Physical and optical properties of mineral dust aerosol during the dust and biomass-burning experiment *J. Geophys. Res.* **113** D00C03

Rocha-Lima A *et al* 2017 A detailed characterization of the Saharan dust collected during the Fennec Campaign in 2011: *in situ* ground-based and laboratory measurements *Atmos. Chem. Phys. Discuss.*

Ryder C L, Highwood E J, Lai T M, Sodemann H and Marsham J H 2013 Impact of atmospheric transport on the evolution of microphysical and optical properties of Saharan dust *Geophys. Res. Lett.* **40** 2433–8

Silva H G, Lopes F, Pereira S, Nicoll K, Barbosa S M, Conceição R, Neves S, Harrison R G and Collares Pereira M 2016 Saharan dust electrification perceived by a triangle of atmospheric electricity stations in Southern Portugal *J. Electrostat.* **84** 106–20

Stein A F, Draxler R R, Rolph G D, Stunder B J B, Cohen M D and Ngan F 2015 NOAA's HYSPLIT atmospheric transport and dispersion modeling system *Bull. Am. Meteor. Soc.* **96** 2059–77

Ulanowski Z, Bailey J, Lucas P W, Hough J H and Hirst E 2007 Alignment of atmospheric mineral dust due to electric field *Atmos. Chem. Phys.* **7** 6161–73

Yang Z, Wang J, Ichoku C, Hyer E and Zeng J 2013 Mesoscale modeling and satellite observation of transport and mixing of smoke and dust particles over northern sub-Saharan African region *J. Geophys. Res. Atmos.* **118** 139–12

Yair Y, Katz S, Yaniv R, Ziv B and Price C 2016 An electrified dust storm over the Negev desert, Israel *Atmos. Res.* **181** 63–71

Weinzierl B *et al* 2017 The saharan aerosol long-range transport and aerosol cloud interaction experiment (SALTRACE): overview and selected highlights *Bull. Am. Meteorol. Soc.* **98** 1427–51